Light-Powered Starter for Micro-Power Boost DC–DC Converter for CMOS Image Sensors

Grzegorz Blakiewicz, Jacek Jakusz, Miron Kłosowski, Waldemar Jendernalik & Stanisław Szczepański

Springer

Springer

Light-Powered Starter for Micro-Power Boost DC–DC Converter for CMOS Image Sensors

Grzegorz Blakiewicz[1] ⬤ · **Jacek Jakusz**[1] ⬤ · **Miron Kłosowski**[1] ⬤ ·
Waldemar Jendernalik[1] ⬤ · **Stanisław Szczepański**[1] ⬤

Abstract

The design of a starter for a low-voltage, micro-power boost DC–DC converter intended for powering CMOS image sensors is presented. A unique feature of the starter is extremely low current, below 1 nA, supplying its control circuit. Therefore, a high-voltage (1.3 V) configuration of series-connected photovoltaic diodes available in a standard CMOS process or a small external LED working in photovoltaic mode can be used as an auxiliary supply for the control circuit. With this auxiliary supply, the starter can generate a starting voltage from 1 to 2.7 V using 50–200 mV supply voltage. The starter was verified by simulations and measurements of a prototype chip fabricated in a standard 180-nm CMOS technology. The results of simulations and tests showed correct operation of the starter in the temperature from 0 to 50 °C and under process parameters variation.

Keywords CMOS · Low voltage · Low power · Boost DC–DC converter ·
Energy harvesting · Image sensor

1 Introduction

Energy available in the environment in the form of light, temperature gradient, electromagnetic waves or vibration can be converted into electric power [11, 13–15, 19, 20] and used to supply micro-sensors. The miniature energy harvesters can generate voltage in the range of 50–400 mV [11, 13–15, 19], which is not sufficient for proper operation of CMOS circuits. For this reason, the voltage generated by the harvesters is boosted to 1 V or more by step-up DC–DC converters. In recent years a number of micro-power step-up switching converters have been developed and implemented

✉ Waldemar Jendernalik
waldemar.jendernalik@pg.edu.pl

1   Faculty of Electronics Telecommunications and Informatics, Gdańsk University of Technology,
Narutowicza 11/12, 80-233 Gdańsk, Poland

Ⓑ Birkhäuser

[1–3, 5, 7, 16–18]. The main limitation of such converters is their inability to self-start at supply voltages as low as 50–400 mV. After starting, the converters can continue operation even at the input voltage reduced to 20 mV [1, 17], because they can generate a proper supply voltage for themselves and for other supplied circuits. The frequently applied solution to the self-start problem is to use an auxiliary starter. In the simplest form, the starter can be a battery [1], but this solution occupies large volume and has a limited life span. The starter can also be a special switching converter designed for operation at extremely low voltage. Such starter provides boosted voltage for the main converter. Unfortunately, the demand for the starter to work at very low voltage results in decreasing its power efficiency and precision of output voltage regulation. For this reason, the starter is only run for a short time to start the main converter. The starter of this type can be based on a JFET [2] or a native MOS [5] transistor with an off-chip transformer. Because JFET and the native MOS transistors can operate at zero gate–source voltage, the start-up is possible even at 20 mV. Because of the need for the off-chip transformer and because JFET is not compatible with CMOS technology, these approaches are limited in application. Another solutions [4, 12, 18] use an LC oscillator based on very-low-threshold-voltage MOS transistors and a Dickson charge pump to generate a sufficiently high start-up voltage.

In the known starter solutions, a voltage source was used as a power source and the main research was focused on reduction of the self-start voltage. In this study, a different approach is applied. Instead of a low-voltage source, a current source with very low current, below 1 nA and voltage of 1.1–1.3 V, is used to power the starter control circuit. Such approach is particularly suitable for sensors exposed to light, because the required current source can be realized as a set of photovoltaic diodes connected in series, which are available in a standard CMOS process [10]. Therefore, the proposed starter can be integrated with a CMOS image sensor.
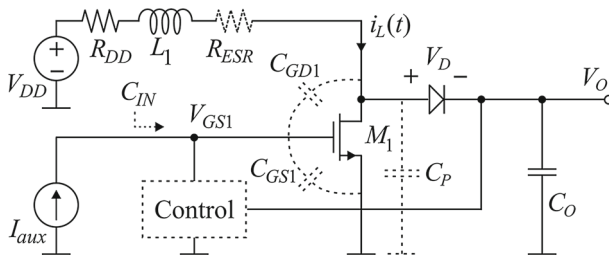
2 Principle of Operation

2.1 Basic Assumptions and Working Conditions

The concept diagram of the proposed starter is shown in Fig. 1. In this starter, a single period of power conversion consists of two cycles. During the first one, the equivalent input capacitance C_{IN} is charged by means of the auxiliary current source I_{aux}. In the next cycle, the transistor M_1 is switched off, by quick discharge of C_{IN}, to generate a boosted voltage at the drain. To initiate operation of the starter, the gate–source voltage V_{GS1} must be increased to

$$V_{\mathrm{GS1}} \cong V_{\mathrm{th}} + \frac{1}{R_{\mathrm{ON1}}} \frac{1}{K_{\mathrm{PN}}(W/L)_1} \tag{1}$$

where V_{th}, $(W/L)_1$, K_{PN} and R_{ON1} are the threshold voltage, the aspect ratio, the transconductance parameter and the required switch-on resistance of M_1, respectively.

Fig. 1 Schematic diagram showing the principle of operation of the starter

Due to a low supply voltage ($V_{DD} < V_{GS1} - V_T$), the MOS transistor model [9] for the triode region is used in (1). When V_{GS1} increases to the value (1), the current $i_L(t)$ flowing through the inductor L_1 reaches its maximum value equal to

$$I_{\max} = \frac{V_{DD}}{R_{ON1} + R_{ESR} + R_{DD}} \tag{2}$$

where R_{ESR} and R_{DD} are the inductor equivalent series resistance and the supply source internal resistance. The current accumulates in the inductor the energy E_L

$$E_L = \frac{1}{2} L_1 I_{\max}^2 = \frac{L_1 V_{DD}^2}{2(R_{ON1} + R_{ESR} + R_{DD})^2} \tag{3}$$

When the switch M_1 opens, the energy (3) is released through the diode and is mainly consumed to charge the output capacitor C_O and the parasitic capacitance C_P. Part of this energy is dissipated in the diode, due to the voltage drop V_D, and is also dissipated in M_1 because of a limited switching-off time and other parasitic effects. Therefore, the energy balance is

$$E_L = E_O + E_P + E_D + E_{M1} = \frac{1}{2} C_O V_O^2 + \frac{1}{2} C_P V_{\text{off}}^2 + E_D + E_{M1} \tag{4}$$

where V_O is the output voltage, V_{off} is the amplitude of the drain voltage pulse after switching off the transistor, and E_D and E_{M1} are the energy dissipated in the diode and in the transistor, respectively. Typical waveforms of the inductor current $i_L(t)$, the voltage drop $v_D(t)$ across the diode and the voltage $V_{\text{off}}(t)$ at the drain of M_1 are depicted in Fig. 2.

Figure 2 shows that while the diode is conducting current, the voltage drop $v_D(t)$ on it and as a consequence voltage on the inductor are almost constant, and therefore, the inductor current $i_L(t)$ decreases linearly in time. Taking this into account, the energy E_D can be estimated as

$$E_D = \int_0^{\Delta t} v_D i_L dt \cong \frac{V_D I_{\max}}{2} \Delta t \cong \frac{V_D I_{\max}}{2} \frac{L_1 I_{\max}}{V_{\text{off}}} \tag{5}$$

where Δt is the duration of the drain voltage pulse $V_{\text{off}}(t)$ and V_D is the maximum voltage drop across the diode. The energy E_{M1} is difficult to calculate, because it
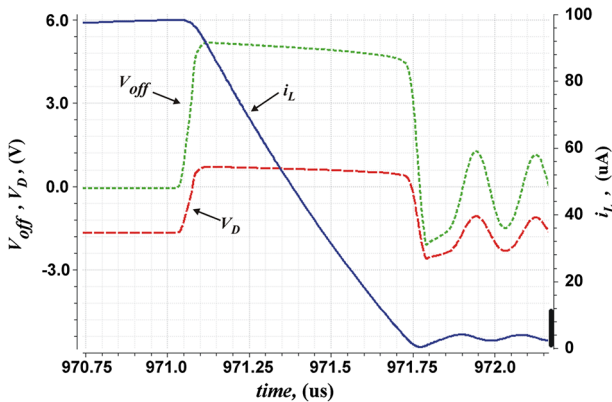
Fig. 2 Waveforms of the inductor current $i_L(t)$, voltage $V_{off}(t)$ at M_1 drain and voltage drop $v_D(t)$ across the diode after switching off M_1 transistor

depends on many factors such as M_1 switching-off time, the ratio of V_{GS1} to V_{th} before M_1 switching-off, R_{ON1}, amplitude of $V_{off}(t)$, oscillations. For this reason, the efficiency factor η is introduced which models the energy loss in the transistor. Using this factor, the loss can be expressed as $E_{M1} = (1 - \eta)E_L$, where the value of η is determined during preliminary simulations based on the energy stored in the inductor and the energy dissipated in the transistor in a single switching cycle, as explained in Sect. 3.2. Based on (3)–(5), and taking into account that $V_{off} = V_O + V_D$, the required inductor current can be estimated as

$$I_{max} \cong \sqrt{\frac{(V_D + V_O)\left[C_O V_O^2 + C_P (V_D + V_O)^2\right]}{L_1[\eta V_O - (1 - \eta)V_D]}} \tag{6}$$

It is assumed that the auxiliary current I_{aux} is used only to initiate the first switch-on of M_1, and the next cycles of charging C_{IN} are supplied using the output voltage V_O. This assumption allows for a reliable start when the starter control circuit is powered from a source with very low current efficiency and accumulated energy, such as a set of serial-connected photovoltaic diodes integrated on a chip. However, the prerequisite for this mode of operation is to meet the following two conditions. First, the maximum inductor current (2) should be greater than (6) to generate the V_O high enough (greater than (1)) to sustain the operation of the starter. Second, the switching period should be greater than the time constant $L_1/(R_{ON1} + R_{ESR} + R_{DD})$; otherwise, the $i_L(t)$ will not reach the required value (6). Thus, the minimum energy for the starter initialization is

$$E_{start} = \frac{1}{2}C_{IN}V_{GS1}^2 \tag{7}$$

where V_{GS1} is such that the current (2) is greater than (6), and $C_{IN} \cong C_{GS1} + C_{GD1}$ because the parasitic capacitances of the transistor M_1 are dominant.
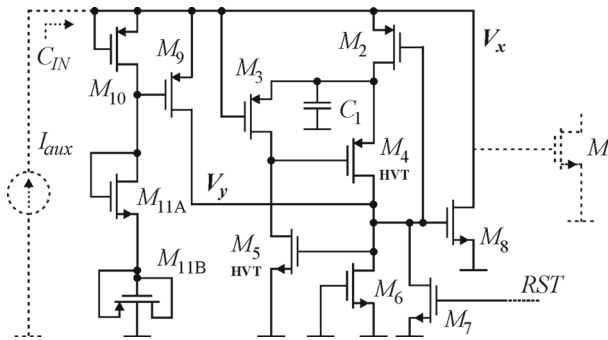
Fig. 3 Relaxation oscillator as a control circuit (HVT devices are 1.8-V transistors with high threshold voltage)

2.2 Relaxation Oscillator

The starter in Fig. 1 needs a control circuit that periodically switches the M_1. To minimize the starting energy, the control circuit should consume as small power as possible. A circuit proposal with such characteristics is shown in Fig. 3. In this configuration, the equivalent capacitance C_{IN} serves as a temporary voltage source supplying the control circuit. Therefore, in ideal conditions, to discharge C_{IN}, no additional energy is required in addition to the energy previously stored in it.

The reuse of energy stored in C_{IN} for the discharging is mainly limited by the static power consumed by the control circuit, because the energy dissipated exactly at the switching transition is desirable since it accelerates the discharging of C_{IN}.

When the circuit is idle, the static power is dissipated as a result of the leakage currents flowing through all the transistors connected between the gate of M_1 and ground. This power can be minimized by using long channel transistors ($L > 1 \, \mu$m) and transistors M4 and M5 with high threshold voltage (HVT) having small leakage current. As a result, the total static current in the proposed circuit is 190 pA at room temperature. The circuit in Fig. 3 together with C_{IN} and I_{aux} acts as a relaxation oscillator. The transistors M_3, M_5 and M_4, M_6 form two cross-coupled inverters functioning as an RS latch. Each inverter is composed of M_4 (M_5) transistor loaded by a very large resistance resulting from M_3 (M_6) leakage current. The transistors sizes are chosen in such a way that M_4 and M_5 are always switched off when the latch is idle. Two transistors M_9 and M_7 are used to set, respectively, high or low voltage levels at the latch output V_y. The circuit composed of M_{10}, M_{11A}, M_{11B} defines the threshold level V_{TH1} of the voltage V_x at which the latch is triggered. Although the threshold V_{TH1} is dependent on temperature and process variation, this solution was chosen because of the very low bias current, which in this case is of utmost important. The influence of the threshold V_{TH1} variation on the operation of the starter will be discussed in Sect. 4. When the V_x reaches the threshold level V_{TH1}, the drain current of M_9 increases and sets the latch output to high. At the same time, M_8 switches on and discharges C_{IN}. It should be noted that without M_2 and C_1, the capacitance C_{IN} could not be discharged completely. The incomplete discharge occurs, because after switching on M_4 (assum-
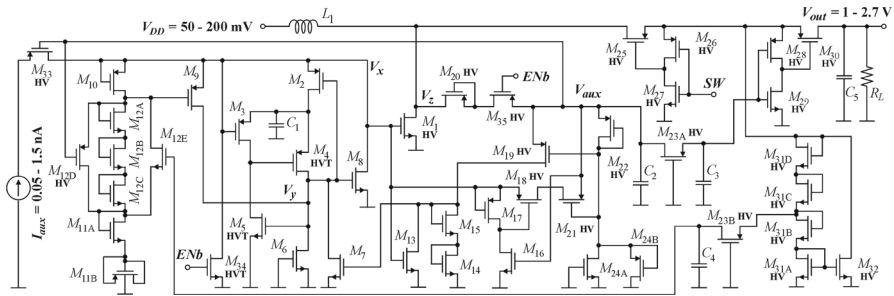
Fig. 4 Complete schematic diagram of the proposed starter (HV are high-voltage 5-V transistors, HVT are 1.8-V transistors with high threshold voltage)

ing that M_2 is shorted) the transistor M_8 forms the diode-connected configuration. As a result, the final minimal voltage V_y can only reach the M_8 threshold voltage and therefore cannot be zeroed. As a consequence, the boosting level of the output voltage is significantly reduced. To avoid such a situation, the temporary voltage source in the form of C_1 is used to provide the gate–source voltage for M_8 high enough to discharge C_{IN} completely. Therefore, M_2 plays two roles: It disconnects C_1 from V_x during the discharge transition, preventing C_1 from complete discharging, and it recharges C_1 to full voltage V_x after discharging C_{IN}. The relaxation oscillator needs periodic resetting of the latch after each state change, which is done by means of M_7 and the signal *RST*.

3 Starter for a Boost DC–DC Converter

3.1 Starter Realization

The proposed starter is only intended for generating the start-up voltage sufficient for a main boost converter. Therefore, after the converter initialization the starter is disabled. The complete schematic of the starter is depicted in Fig. 4. The circuit consists of the following functional blocks: the relaxation oscillator (M_2–M_{12}, C_1), the feedback supplying circuit (C_2, M_{16}–M_{18}, M_{21}, M_{22}, M_{24}), the MOS rectifiers (M_{20}, M_{25}), the voltage limiter (M_{31A}–M_{31D}, M_{32}) and the disabling circuit (M_{34}, M_{35}) which switches off the starter after the boost converter initialization. To limit the number of off-chip components, the starter shares L_1 with the boost converter.

When the relaxation oscillator switches off M_1 for the first time, a positive pulse voltage V_z at the drain is generated. This pulse switches on the rectifiers M_{20} and M_{25} (initially the signal *SW* is low). During the first switching, M_{30} is turned off because its gate is connected to source by M_{28}. M_{30} is switched on after the delay resulting from charging C_3 by means of M_{23A}. Therefore, the large capacitor C_5 and the other supplied circuits are disconnected during this period. As a result, most of the energy accumulated in the inductor L_1 is released through M_{20} and M_{35} to the capacitor C_2. Since C_2 has relatively small capacitance, the voltage across C_2 quickly rises above the latch threshold. From this moment, the starter is able to power itself using C_2 as

an auxiliary voltage source for I_{aux} generation. The transistors M_{21}, M_{22}, M_{24} form a current source which takes over the role of the source I_{aux}. M_{16}–M_{18} are used to prevent a feedforward flow of the I_{aux} during the first switching of M_1. In this period, M_{18} is switched off, because its gate is connected to the source by the leakage current of M_{17}. When the starter switches to the auxiliary source C_2, M_{18} is turned on by M_{16}, which connects the gate of M_{18} to ground. At the same time, the source I_{aux} is disconnected, by turning off M_{33}, to prevent energy losses.

For a proper operation, the relaxation oscillator needs cyclic resetting. This task is accomplished by M_7, M_{13}–M_{15} and M_{19}. When the voltage V_{aux} on C_2 reaches a sufficient level, M_7 switches on and resets the latch output V_y to zero. From this moment, the voltage V_x may increase and C_{IN} may be charged again. M_{13} is used to disable M_7 and cancel the resetting of the latch to enable next switching of the relaxation oscillator.

To minimize the starting energy, the threshold level of the latch is modulated. During the first switching on of M_1, the threshold voltage of the latch is set to the minimum, defined by M_{11A}, M_{11B}, since M_{12D} is switched on ($V_{aux} = 0$). This voltage is such that the starter generates energy to charge the capacitor C_2 to the required minimal level (1). Such small energy is not sufficient to charge a much larger capacitor C_5 to the level required by a boost converter. Therefore, during next cycles of oscillation the latch threshold voltage is increased, by switching off M_{12D}, to the level defined by M_{11A}, M_{11B} and M_{12A}–M_{12C}.

During the initial oscillations, it is not possible to precisely control voltages V_{aux} and V_{out} which may result in exceeding permissible voltage limits. To protect the circuit from damage by too high voltage, the voltage limiter composed of M_{31}–M_{32} is applied. When the amplitude of V_z pulse exceeds the permissible value, M_{12E} and M_{32} are switched on to reduce the latch threshold voltage, V_{aux}, and V_{out}.

After several cycles of oscillation, when V_{out} reaches the required start-up voltage for a proper operation of the boost converter, the starter is disabled by pulling the signal ENB to high. At the same time, the transistor M_{25} changes its role from the rectifier to a switch controlled by the pulse-width-modulated signal SW, which is generated by a circuit controlling the boost converter.

The exemplary waveforms illustrating the starter operation are presented in Fig. 5. The bottom waveform shows voltage V_x across C_{IN}. During the initialization period, the voltage gradually increases until it reaches, at about 420 µs, the latch threshold level of 0.81 V. After the first switching, the threshold is increased to about 1.2 V. From this moment, relaxation oscillations begin. As shown in the top and middle plots, the first switching charges C_2 to about $V_{aux} = 2.55$ V and C_5 to $V_{out} = 20$ mV. After about 1.7 ms, both voltages reach the final values $V_{aux} = 2.3$ V and $V_{out} = 2$ V. It should also be noted that after 1.7 ms, the latch threshold voltage is reduced to about 1 V to limit the output voltage. In most working conditions, the first switching is sufficient to charge C_2 to a high enough level, but if this action fails, the switching will resume automatically.
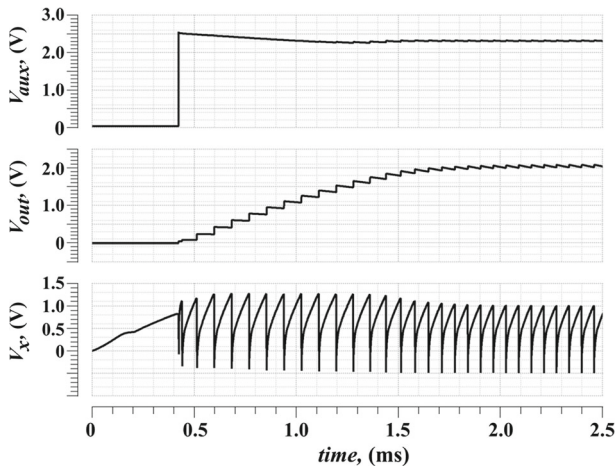
Fig. 5 Exemplary waveforms of the starter voltages: V_{aux}, V_{out} and V_x

3.2 Design Procedure

The design procedure is explained based on two variants of the starter: (1) with the minimal starting energy and (2) with the lowest start-up voltage. The starter is designed for a boost converter that requires the start-up voltage $V_{\text{out}} \geq 1$ V. The AMS 180-nm standard CMOS technology was selected for both variants of the project. To make the preliminary calculations, the following parameters were assumed: $V_{\text{DD}} = 50$ mV, $R_{\text{DD}} = 5\,\Omega$, $L_1 = 800\,\mu\text{H}$, $R_{\text{ESR}} = 0.35\,\Omega$. The remaining parameters were estimated as follows. The capacitance $C_5 = 10$ nF was selected to achieve V_{out} voltage ripple less than 20 mV$_{\text{pp}}$. The C_2 equal to 120 pF was chosen to obtain V_{aux} voltage ripple less than 100 mV which guarantees correct operation of the relaxation oscillator. The capacitance $C_1 = 0.6$ pF is ten times larger than the input capacitance of M_8, to keep the M_8 gate–source voltage high enough to discharge C_{IN} completely. The efficiency factor $\eta = 1 - E_{M1}/E_L = 0.7$ was determined based on the energy dissipated in the transistor E_{M1} and the energy stored in the inductor E_L, where both energies were calculated by simulation for a single switching period. The determined maximum voltage drop on the rectifier M_{25} was $V_D = 0.9$ V.

As explained in the previous section, two threshold levels are used in the latch. The first threshold level V_{TH1} should guarantee generation of enough energy to charge C_2 to voltage greater than (1), while the second threshold level V_{TH2} should be sufficient to charge $C_2 + C_5$ and provide enough power for the load R_L. After the first switching, the required gate–source voltage (1) is generated by the feedback supplying circuit (M_{16}–M_{18}, M_{21}, M_{22}, M_{24}), which needs at least 50 mV voltage drop for proper operation. Therefore, the minimal initial voltage (1) must be greater by this value. The first variant of the starter, with the minimal starting energy, was design using (1), (2), (6) and finding dimensions W_1 and L_1 of the transistor M_1 for which the energy (7) is minimal. It is assumed that $C_{\text{IN}} \cong W_1 L_1 C_{ox} + C_1$, $C_P = 2W_1 C_{ov} + C_x$ where C_{ox} is the capacitance per unit area of M_1 gate oxide, C_{ov} is the overlap

Table 1 Parameters of the starter in Fig. 4

Device: μm/μm	Device: μm/μm	Device: μm/μm
M_3: 10/2	M_{17}: 10/0.18	M_{24B}: 10/1
M_4: 5/2	M_{18}: 1/10	M_{25}: 50/0.5
M_6: 5/2	M_{19}: 5/2	M_{26}: 10/1
M_7: 2/5	M_{20}: 2/0.5	M_{27}: 5/1
M_8: 10/2	M_{21}: 20/1	M_{30}: 50/1
M_{10}: 12/2	M_{22}: 2/10	M_{30A-D}: 5/1
M_{11B}: 3/2	M_{23A}: 1/10	M_{32}: 500/0.7
M_{12D}: 1/4	M_{23B}: 1/10	$C_1 = 0.6$ pF
M_{16}: 2/10	M_{24A}: 10/1	$C_{3,4} = 1$ pf
Other transistors: 2/2	M_1: 500/0.7 for min start-up voltage	M_1: 1500/0.7 for min start-up energy

capacitance per channel unit width, and C_x is the capacitance resulting from M_{20}, M_{25} ($C_x \cong 0.4$ pF). In this case, for the worst technology corner ($V_T \cong 520$ mV, $K_{PN} \cong 100$ μA/V^2, $C_{ox} \cong 2.5$ fF/μm^2, $C_{ov} \cong 0.5$ fF/μm^2) the required first threshold voltage is $V_{TH1} \cong 800$ mV, and the transistor dimensions are $W_1 \cong 500$ μm and $L_1 = 0.7$ μm.

The second variant of the starter, with the lowest start-up voltage, was calculated using the same set of equations, but finding the transistor dimensions for which the gate–source voltage (1) is minimal. In this case, the optimal parameters are as follows: $V_{TH1} \cong 650$ mV, $W_1 \cong 1500$ μm and $L_1 = 0.7$ μm.

The second threshold level V_{TH2} depends on the required charging rate of C_5 and the load resistance R_L. The greater the V_{TH2} is, the faster the output voltage V_{out} reaches its final value. Since the maximum value of V_{TH2} is limited by V_{aux}, which is in the range of 1.6–2.4 V, with a small margin of safety it was assumed that $V_{TH2} = 1.5V_{TH1}$. The effects of V_{TH1} and V_{TH2} changes due to temperature and process variations are discussed in Sect. 4.1. The complete set of circuit parameters is listed in Table 1

4 Analysis of Working Conditions and Technology Nonidealities

4.1 Technology Corners and Temperature Variation

Due to the use of leakage currents for biasing of devices, the influence of technology corners and temperature variation on the starter operation is examined. Five corners are specified for AMS (austriamicrosystems AG) 180-nm CMOS technology: TM, WP, WS, WO and WZ, meaning, respectively, the typical mean values, worst-case power, worst-case speed, worst-case one and worst-case zero.

For a proper operation of the starter, both transistors M_4 and M_5 must always be switched off when the latch is idle. To meet such a condition, M_3 leakage current must always be greater than M_5 leakage current. Similarly, the sum of M_4 and M_9 leakages should be greater than the sum of M_6 and M_7 leakages. Such conditions are

satisfied by using HVT transistors M_4 and M_5 and proper sizing of the other devices. It is also required that the threshold voltages V_{TH1} and V_{TH2} of the latch were as constant as possible and greater than (1). These voltages, in the circuit in Fig. 4, can be approximated as

$$V_{TH1} = V_{DS11A} + V_{SB11B} + V_{th9} \tag{8a}$$

$$V_{TH2} = V_{DS11A} + V_{SB11B} + V_{DS12A} + V_{DS12B} + V_{DS12C} + V_{th9} \tag{8b}$$

where V_{DS11A}, V_{DS12A}–V_{DS12C}, are the drain–source voltages of M_{11A} and M_{12A}–M_{12C}, respectively, V_{SB11B} is the source–body voltage of M_{11B}, whereas V_{th9} is the threshold voltage of M_9. The transistors M_{11A} and M_{11B} (M_{12A}–M_{12C}) are biased by the leakage current of the p-channel transistor M_{10}, which can be approximated by [9]

$$I_{leak10} \cong \left(\frac{W}{L}\right)_{10} I_{O10} \left(\frac{T}{T_0}\right)^2 e^{-\frac{V_{th10}}{nV_T}} \tag{9}$$

where I_{O10} and n are technology parameters, V_T is the thermal voltage, and T_O is a reference temperature. On the other hand, the drain–source voltage of each transistor M_{11A}, M_{12A}–M_{12C} working in the subthreshold region is

$$V_{DSN} \cong V_{thN} + nV_T \ln(I_{leak10}) - nV_T \ln\left[\left(\frac{W}{L}\right)_N I_{ON} \left(\frac{T}{T_O}\right)^2\right] \tag{10}$$

Taking into account the leakage current (9), the drain–source voltage can be determined as

$$V_{DSN} \cong V_{thN} - V_{th10} + nV_T \ln\left[\left(\frac{W}{L}\right)_{10} I_{O10} \Big/ \left\{\left(\frac{W}{L}\right)_N I_{ON}\right\}\right] \tag{11}$$

The expressions (11), (8a) and (8b) show that the latch thresholds depend mainly on the difference between the threshold voltages V_{thN} and V_{th10} of the n-channel (M_{11A}, M_{12A}–M_{12C}) and p-channel (M_{10}) transistors. Because the temperature coefficients of both voltages V_{thN} and V_{th10} are similar, the change of voltage (11) with temperature is reduced.

Figure 6 shows the simulations results of V_{TH1} and V_{TH2} changes with temperature and corners. For TM corner, V_{TH1} varies from 920 mV to 860 mV for the temperature from 0 to 70 °C. The total variation of V_{TH1}, including all the corners and temperature change, is 820–946 mV. As explained in Sect. 3.1, the first threshold level V_{TH1} is used during the start-up of the relaxation oscillator, when it is powered from the photovoltaic diodes. The starter is designed to be powered from the photovoltaic diodes in the configuration described in [10] or a small external LED working in photovoltaic mode. In both cases, the generated voltage is in the range of 1.1–1.3 V, which guarantees proper start-up of the relaxation oscillator.
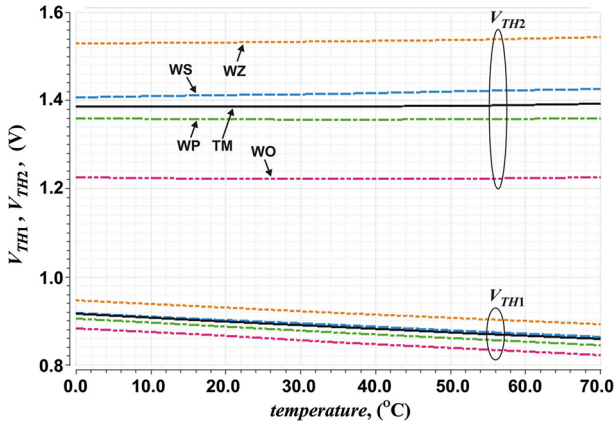
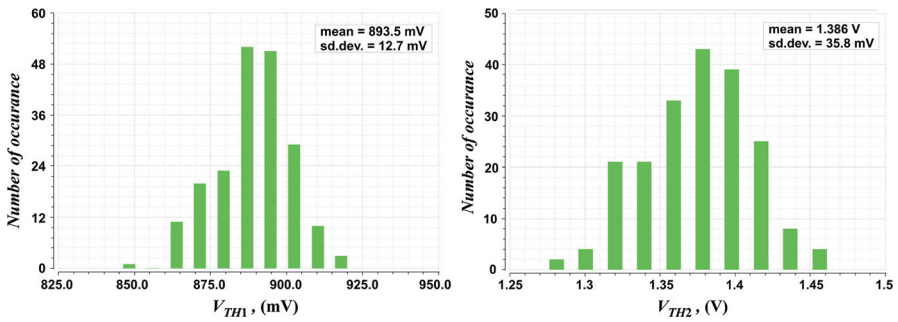**Fig. 6** V_{TH1} and V_{TH2} variation with temperature and corners

Fig. 7 Monte Carlo simulation results of V_{TH1} and V_{TH2} for TM corner at 27 °C

Figure 6 shows that under the same conditions, the second threshold voltage V_{TH2} changes from 1.386 to 1.394 V for TM corner and from 1.2 to 1.544 V for all the corners and temperature range 0–70 °C. The V_{TH2} is used to reduce the charging time of the capacitor C_5, and therefore, its relatively large variation has less impact on the starter operation. Because after starting, the oscillator is powered from the auxiliary source V_{aux} higher than 1.6 V, the operation of the oscillator is sustained regardless of changes in V_{TH2}. The changes in V_{TH1} and V_{TH2} caused by mismatch of the transistors dimensions and variation of technology parameters achieved with 200 runs of the Monte Carlo simulations are illustrated in Fig. 7 for TM corner and temperature 27 °C. The complete set of simulation results for all the corners and temperatures 0, 27, 70 °C is presented in Table 2. Both threshold voltages are within the range of acceptable values (0.8 V $< V_{TH1} <$ 1.1 V and $V_{TH2} <$ 1.6 V).
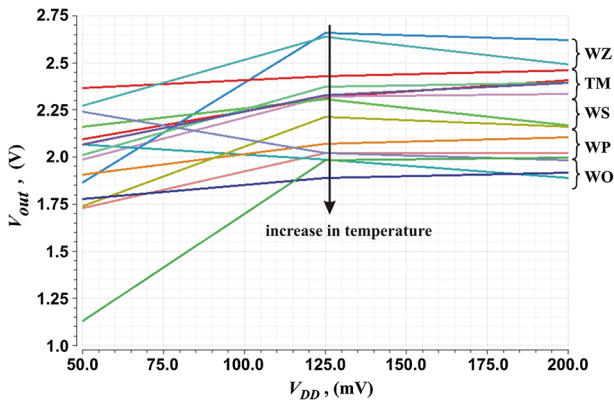
4.2 Output Voltage Variation

As the proposed starter is to be used only for a short initialization period to start a boost converter, a simple mechanism for controlling the output voltage V_{out} is applied.

Ⓑ Birkhäuser

Table 2 Summary of the Monte Carlo simulation of V_{TH1} and V_{TH2}

| Corner	V_{TH1} (mV)			V_{TH2} (V)		
	0 °C	27 °C	70 °C	0 °C	27 °C	70 °C
TM	M = 916.6	M = 893.5	M = 859.6	M = 1.385	M = 1.386	M = 1.392
	SD = 11.8	SD = 12.7	SD = 13.1	SD = 0.0345	SD = 0.0358	SD = 0.0362
WP	M = 906.0	M = 881.5	M = 845.0	M = 1.360	M = 1.357	M = 1.359
	SD = 12.1	SD = 12.8	SD = 13.2	SD = 0.035	SD = 0.0367	SD = 0.0352
WS	M = 918.8	M = 897.8	M = 865.0	M = 1.406	M = 1.413	M = 1.426
	SD = 11.5	SD = 11.7	SD = 11.9	SD = 0.0335	SD = 0.0343	SD = 0.0348
WO	M = 882.7	M = 859.3	M = 823.6	M = 1.225	M = 1.223	M = 1.226
	SD = 11.6	SD = 11.7	SD = 13.2	SD = 0.034	SD = 0.036	SD = 0.0368
WZ	M = 947.5	M = 925.3	M = 893.9	M = 1.528	M = 1.532	M = 1.541
	SD = 11.8	SD = 12.3	SD = 13.6	SD = 0.036	SD = 0.0365	SD = 0.0372

M mean value, *SD* standard deviation

Fig. 8 V_{out} as a function of V_{DD} for all combinations of temperatures 0 °C, 27 °C and 70 °C and corners TM, WP, WS, WO and WZ

For relatively small supply voltages $V_{DD} < 50$ mV, the output voltage is unregulated, whereas for higher voltages the output is limited by the circuit composed of M_{31A}–M_{31D}, M_{32} and M_{12E}. The characteristics of the output voltage are shown in Fig. 8. The curves shown refer to all combinations of the five corners TM, WP, WS, WO and WZ and three temperatures 0 °C, 27 °C and 70 °C. The output voltage V_{out} ranges from 1.12 to 2.7 V for V_{DD} from 50 to 200 mV, which guarantees a reliable start of the converter.

To determine the V_{out} changes caused by devices mismatch and process variation, 200 iterations of Monte Carlo simulations were performed. The results for TM corner and $V_{DD} = 50$ mV are illustrated in Fig. 9 for 0 °C and 70 °C, whereas a summary of
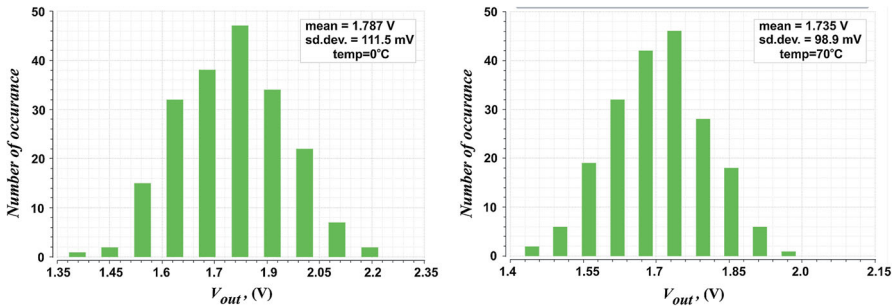
Fig. 9 Monte Carlo simulation results of V_{out} for TM corner at 0 °C and 70 °C

Table 3 Summary of the Monte Carlo simulation of V_{out} at $V_{\text{DD}} = 50$ mV

| Corner	V_{out} (V)		
	0 °C	27 °C	70 °C
TM	$M = 1.787$ $SD = 0.112$	$M = 1.772$ $SD = 0.105$	$M = 1.735$ $SD = 0.0989$
WP	$M = 1.772$ $SD = 0.109$	$M = 1.755$ $SD = 0.1$	$M = 1.715$ $SD = 0.099$
WS	$M = 1.12$ $SD = 0.117$	$M = 1.113$ $SD = 0.105$	$M = 1.08$ $SD = 0.1$
WO	$M = 2.05$ $SD = 0.128$	$M = 2.025$ $SD = 0.121$	$M = 1.98$ $SD = 0.115$
WZ	$M = 2.35$ $SD = 0.113$	$M = 2.37$ $SD = 0.105$	$M = 1.89$ $SD = 0.099$

M mean value, SD standard deviation

the results for all the corners at 0 °C, 27 °C and 50 °C is given in Table 3. The output voltage varies from 1.08 to 2.37 V, and therefore, a reliable start of the converter is possible. The main reasons for the output voltage changes are the changes in the threshold voltages V_{TH1}, V_{TH2} and the switch-on resistance of M_1 (R_{ON1} in (1)). The V_{out} variation could be reduced by means of negative feedback; however, in such a case it would not be possible to achieve very low auxiliary current $I_{\text{aux}} < 1$ nA due to the complexity of the feedback circuit.

4.3 Auxiliary Current Variation

The auxiliary current I_{aux} is mainly used for charging the input equivalent capacitance C_{IN}. Only a relatively small fraction of this current is consumed by the leakage current of the control circuit. The plots of the minimum I_{aux} necessary to initiate the starter as a function of temperature and corners are presented in Fig. 10. For the V_{DD} equal to 50 mV and all the corners, the current is below 1 nA if temperature is lower than 57 °C, while for TM corner and room temperature the current is 190 pA. Such a low
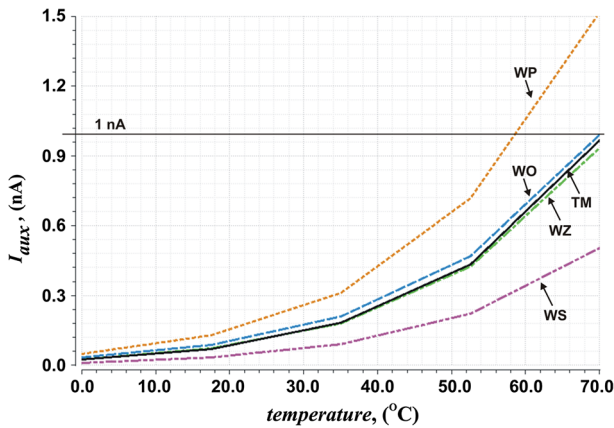
Fig. 10 The minimum I_{aux} necessary to initiate the starter as a function of temperature and corners
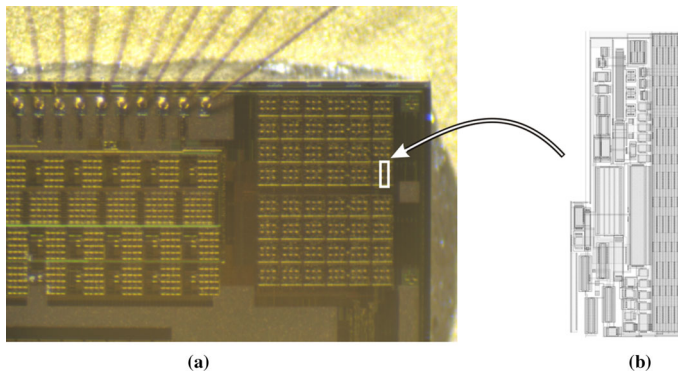
Fig. 11 a Micro-photograph of the chip portion containing the starter. **b** Design of the starter layout (21 μm × 110.7 μm)

current value allows the use of on-chip photovoltaic diodes or small external LED diode in photovoltaic mode.

5 Measurement of a Prototype Starter

The starter from Fig. 4 in the version with minimal starting energy was selected for fabrication in a standard AMS 180-nm CMOS technology. The designed starter's layout and the micro-photograph of the chip portion containing the starter are shown in Fig. 11. The complete starter without bonding pads occupies 2325 μm² of the chip area. The L_1, C_2, C_5 and R_L were implemented as external components with values 820 μH, 120 pF, 10 nF and 1 MΩ, respectively. In the test setup (Fig. 12), the main power source V_{DD} was a photodiode BPW20RF (manufactured by Vishay) shunted by the capacitor C_D with 3.3 μF value. The auxiliary current I_{aux} was generated by a light-emitting diode (LED) working in photovoltaic mode. We used a small green
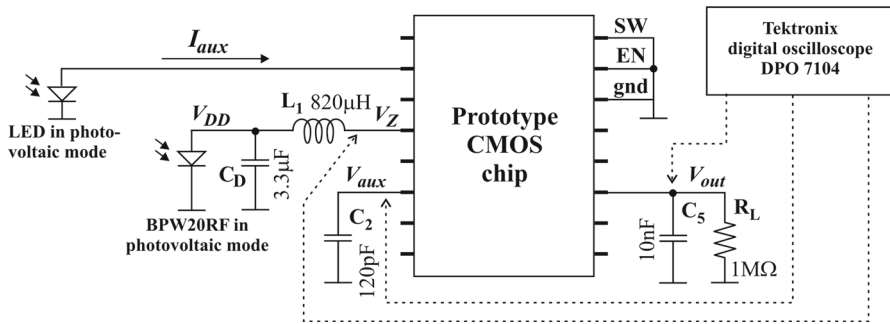
Fig. 12 The test setup

**Table 4** Measured V_{out} and V_{aux} as a function of V_{DD}

		V_{DD} (mV)	50	80	100	150	200
0 °C	V_{out} (V)		1.61	2.32	2.43	2.60	2.69
	V_{aux} (V)		1.42	2.25	2.35	2.53	2.61
27 °C	V_{out} (V)		1.39	2.24	2.35	2.55	2.62
	V_{aux} (V)		1.13	1.92	2.05	2.21	2.35
50 °C	V_{out} (V)		1.15	2.08	2.12	2.18	2.25
	V_{aux} (V)		1.02	1.91	2.02	2.05	2.15

LED with 1.1 V open circuit voltage and 1 nA short-circuit current at 1 klux. Using the configuration in Fig. 12, the relation between V_{DD}, V_{out} and V_{aux} was measured. The V_{DD} was changed by increasing illuminance of incident light. The results of measurements taken for V_{DD} changed from 50 mV to 200 mV are presented in Table 4. The value of the auxiliary current I_{aux} supplying the starter ranges from 120 pA at 0 °C to 0.8 nA at 50 °C. The current measured at room temperature (27 °C) is 240 pA.

Figure 13 shows captured waveforms of V_{out}, V_{aux} and V_Z for $V_{DD} = 50$ mV. It is seen that the first pulse of V_Z charges C_2 to $V_{aux} > 1.9$ V, which ensures correct operation of the relaxation oscillator. At the same time, as shown in Fig. 13b, the voltage V_{out} is delayed and limited in amplitude to 400 mV. During the successive switching of M_1, the V_{out} increases gradually to the final value of 1.39 V.

6 Comparison

Most of the starters described in the literature are designed to achieve the lowest possible start-up voltage, and therefore, comparison of the starter proposed in this paper is difficult. Two groups of the starters are compared: the starters using an auxiliary voltage source [1, 3, 7] and the starter using a single low-voltage source shared with the boost converter [17]. A summary of the most important parameters of the selected starters is given in Table 5. The solution in [1] requires at least 600 mV to start-up and consumes 1.1 μW of quiescent power, which means 1.8 μA inrush current. The starter [3] at the same voltage needs at least 2 μW, which results in 3.3 μA inrush
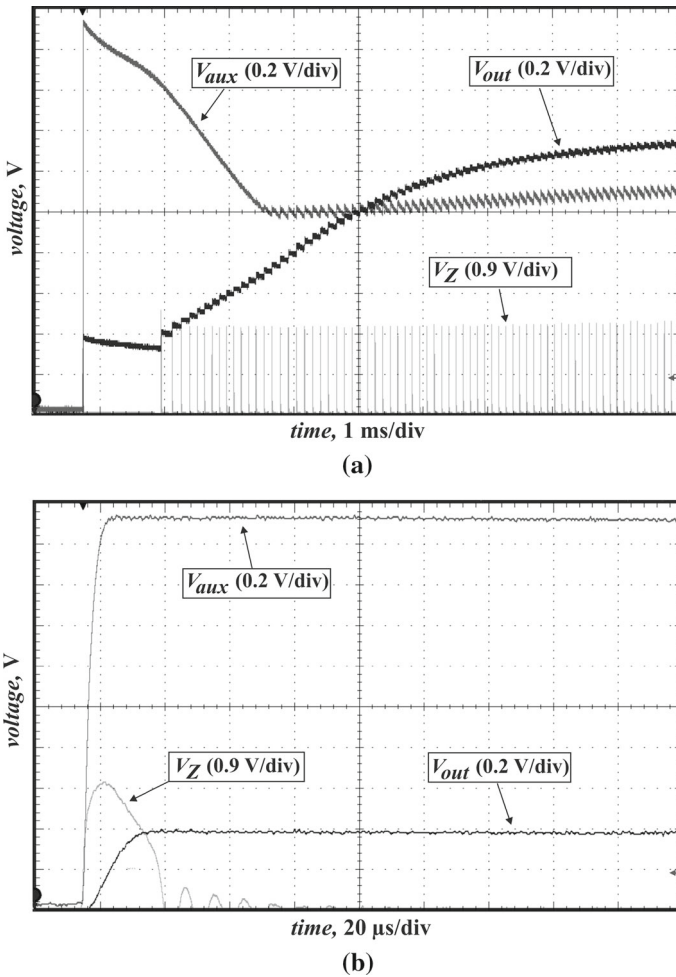
Fig. 13 Oscilloscope measurements of waveforms: V_{out}, V_{aux} and V_Z: **a** start-up after applying $V_{DD} = 50$ mV, **b** enlarged initial part of V_{out}, V_{aux} and V_Z waveforms

current. The control circuit used in the starter [7] requires at least 1 V and consumes 160 nW of power, and therefore, it requires 160 nA of inrush current. The converter in [17] can start up by itself due to the application of a MOS transistor with a low threshold voltage. During the start-up period, 1.3 μW of power is consumed at 35 mV (37 μA inrush current). The proposed starter consumes auxiliary current in the range from 120 pA (0 °C) to 0.8 nA (50 °C) at the starting voltage in the range from 970 mV to 850 mV, and therefore, the static power consumed varies from 0.117 nW to 0.68 nW.

Table 5 Performance comparison of selected starters

References	[1]	[3]	[7]	[17]	This work
Start-up voltage, mV	600	600	1000	35	820–946
Inrush current, nA	1800	3300	160	37000	0.12–0.8
Quiescent power	1.1 μW	2.0 μW	160 nW	1.3 μW	0.12–0.68 nW
Start-up time, ms	na	na	na	na	1.4–10
Switching frequency	0.044–5 MHz	42–320 kHz	15 kHz	1–100 kHz	6.5–50 kHz
Output voltage, V	1	0.9	1.9	1	1–2.7
CMOS technology	130 nm	350 nm	180 nm	130 nm	180 nm

7 Conclusion

In this paper, the starter able to generate a starting voltage in the range from 1 to 2.7 V at a supply voltage from 50 to 200 mV is presented. The starter is designed for a low-voltage, micro-power boost DC–DC converter intended for powering CMOS image sensors. A special feature of the proposed starter is extremely low current, below 1 nA, supplying its controller. Due to this, the controller can be powered from a high-voltage (1.3 V) configuration of series-connected photovoltaic diodes available in a standard CMOS process [10]. Therefore, the proposed solution is suitable for all kinds of image sensors, e.g., imagers, vision chips [6, 8] implemented in CMOS technologies. The very low current supplying the controller was achieved by using a simple relaxation oscillator biased by the leakage current of MOS transistors. The performed simulations have shown that despite the use of such a simple solution, the starter works correctly. It was demonstrated that the starter can be designed in such a way to operate properly under temperature changes in the range of 0–50 °C and process variation. The starter was verified using a prototype chip fabricated in 180-nm CMOS technology. The starter output voltage measured at 0 °C, 27 °C and 50 °C is in the range of 1.1–2.7 V, whereas the controller supply current is within the range of 0.12–0.8 nA.

References

1. E. Carlson, K. Strunz, B. Otis, A 20 mV input boost converter with efficient digital control for thermo-electric energy harvesting. IEEE J. Solid-State Circuits **45**, 741–750 (2010). https://doi.org/10.1109/JSSC.2010.2042251
2. J. Damaschke, Design of a low-input-voltage converter for thermoelectric generator. IEEE Trans. Ind. Appl. **33**, 1203–1207 (1997). https://doi.org/10.1109/28.633797

3. I. Doms, P. Merken, R. Mertens, C. Van Hoof, Integrated capacitive power-management circuit for thermal harvesters with output power 10 to 1000 μW, in *Digest of Technical Papers IEEE International Solid-State Circuits Conference (ISSCC)* (2009), pp. 300–301. https://doi.org/10.1109/isscc.2009.4977427

4. H. Fuketa, S. O'uchi, T. Matsukawa, Fully integrated, 100-mV minimum input voltage converter with gate-boosted charge pump kick-started by LC oscillator for energy harvesting. IEEE Trans. Circuits Syst. II Express Briefs **64**, 392–396 (2017). https://doi.org/10.1109/tcsii.2016.2573382

5. J.-P. Im, S.-W. Wang, S.-T. Ryu, G.-H. Cho, A 40 mV transformer-reuse self-startup boost converter with MPPT control for thermoelectric energy harvesting. IEEE J. Solid-State Circuits **47**, 3055–3067 (2012). https://doi.org/10.1109/JSSC.2012.2225734

6. W. Jendernalik, G. Blakiewicz, J. Jakusz, S. Szczepański, An analog sub-miliwatt CMOS image sensor with pixel-level convolution processing. IEEE Trans. Circuits Syst. I Reg. Pap. **60**, 279–289 (2013). https://doi.org/10.1109/tcsi.2012.2215803

7. J. Katic, S. Rodriguez, A. Rusu, A dual-output thermoelectric energy harvesting interface with 86.6% peak efficiency at 30 μW and total control power of 160 nW. IEEE J. Solid-State Circuits **51**, 189–204 (2016). https://doi.org/10.1109/jssc.2016.2561959

8. M. Kłosowski, W. Jendernalik, J. Jakusz, G. Blakiewicz, S. Szczepański, A CMOS pixel with embedded ADC, digital CDS and gain correction capability for massively parallel imaging array. IEEE Trans. Circuits Syst. I Reg. Pap. **64**, 38–49 (2017). https://doi.org/10.1109/tcsi.2016.2610524

9. K.R. Laker, W.M.C. Sansen, *Design of Analog Integrated Circuits and Systems* (McGraw-Hill, New York, 1994)

10. M.K. Law, A. Bermak, High-voltage generation with stacked photodiodes in standard CMOS process. IEEE Electron Device Lett. **31**, 1425–1427 (2010). https://doi.org/10.1109/LED.2010.2075910

11. V. Leonov, T. Torfs, P. Fiorini, C. Van Hoof, Thermoelectric converters of human warmth for self-powered wireless sensor nodes. IEEE Sens. J. **5**, 650–657 (2007). https://doi.org/10.1109/JSEN.2007.894917

12. B. Lim, J. Seo, S. Lee, A Colpitts oscillator-based self-starting boost converter for thermoelectric energy harvesting with 40-mV startup voltage and 75% maximum efficiency. IEEE J. Solid-State Circuits **53**, 3293–3302 (2018). https://doi.org/10.1109/JSSC.2018.2863951

13. L. Liu, J. Mu, N. Ma, W. Tu, Z. Zhu, Y. Yang, An ultra-low-power integrated RF energy harvesting system in 65-nm CMOS process. Circuits Syst. Signal Process. **35**, 421–441 (2016). https://doi.org/10.1007/s00034-015-0092-7

14. R.D. Prabha, G.A. Rincon-Mora, CMOS photovoltaic-cell layout configurations for harvesting microsystems, in *Proceedings of International Midwest Symposium on Circuits and Systems (MWSCAS)* (2013), pp. 368–371. https://doi.org/10.1109/mwscas.2013.6674662

15. Y. Ramadass, A. Chandrakasan, An efficient piezoelectric energy harvesting interface circuit using a bias-flip rectifier and shared inductor. IEEE J. Solid-State Circuits **45**, 189–204 (2010). https://doi.org/10.1109/JSSC.2009.2034442

16. Y. Ramadass, A. Chandrakasan, A battery-less thermoelectric energy harvesting interface circuit with 35 mV startup voltage. IEEE J. Solid-State Circuits **46**, 333–341 (2011). https://doi.org/10.1109/JSSC.2010.2074090

17. Y.-K. The, P.K.T. Mok, Design of transformer-based boost converter for high internal resistance energy harvesting sources with 21 mV self-startup voltage and 74% power efficiency. IEEE J. Solid-State Circuits **49**, 2694–2704 (2014). https://doi.org/10.1109/JSSC.2014.2354645

18. P.-S. Weng, H.-Y. Tang, P.-C. Ku, L.-H. Lu, 50 mV-input batteryless boost converter for thermal energy harvesting. IEEE J. Solid-State Circuits **48**, 1031–1041 (2013). https://doi.org/10.1109/JSSC.2013.2237998

19. Y. Yang, X.-J. Wei, J. Liu, Suitability of a thermoelectric power generator for implantable medical electronic devices. J. Phys. D Appl. Phys. **40**, 5790–5800 (2007). https://doi.org/10.1088/0022-3727/40/18/042

20. Y. Zhang, F. Zhang, Y. Shakhsheer, J.D. Silver, A. Klinefelter, M. Nagaraju, J. Boley, J. Pandey, A. Shrivastava, E.J. Carlson, A. Wood, B.H. Calhoun, B.P. Otis, A batteryless 19 μW MICS/ISM-band energy harvesting body sensor node SoC for ExG applications. IEEE J. Solid-State Circuits **48**, 199–213 (2013). https://doi.org/10.1109/JSSC.2012.2221217

Ⓑ Birkhäuser